

TOPICAL REVIEW

Elasto-capillarity: deforming an elastic structure with a liquid droplet

B Roman and J Bico

Physique et Mécanique des Milieux Hétérogènes, ESPCI-ParisTech, UMR CNRS 7636,
Paris 6 & Paris 7 Universities, 10 rue vauquelin, 75 005 Paris, France

E-mail: benoit@pmmh.espci.fr and jbico@pmmh.espci.fr

Received 19 July 2010, in final form 28 September 2010

Published 16 November 2010

Online at stacks.iop.org/JPhysCM/22/493101

Abstract

Although negligible at macroscopic scales, capillary forces become dominant as the sub-millimetric scales of micro-electro-mechanical systems (MEMS) are considered. We review various situations, not limited to micro-technologies, where capillary forces are able to deform elastic structures. In particular, we define the different length scales that are relevant for 'elasto-capillary' problems. We focus on the case of slender structures (lamellae, rods and sheets) and describe the size of a bundle of wet hair, the condition for a flexible rod to pierce a liquid interface or the fate of a liquid droplet deposited on a flexible thin sheet. These results can be generalized to similar situations involving adhesion or fracture energy, which widens the scope of possible applications from biological systems, to stiction issues in micro-fabrication processes, the manufacturing of 3D microstructures or the formation of blisters in thin film coatings.

(Some figures in this article are in colour only in the electronic version)

Contents

1. Introduction: capillary forces at small scales	1
2. Elasto-capillary length	3
2.1. Capillarity and bulk elasticity	3
2.2. Slender structures: elasto-capillary length	3
2.3. Adhesion boundary conditions in elasto-capillary problems	4
3. Wet hairs	5
4. Piercing hairs	7
5. Sheets and surface tension	8
6. Conclusion and prospectives	11
Acknowledgments	12
Appendix	12
References	12

1. Introduction: capillary forces at small scales

The effects of a fluid on human-built structures are generally due to the fluid's weight or its flow. For example, hydrostatic

pressure limits the size of fuel tanks and may induce the collapse of immersed pipelines. Similarly the inertia of a fluid in motion induces drag or lift forces (e.g. the destruction of the Tacoma Narrows bridge). Flows in a confined environment also produce viscous stresses that may be strong enough to deform solid materials (e.g. in bearing systems). However, the growing interest for micro-devices of the size of an ant has brought attention to another type of interaction that can have a strong impact even when the fluid is at rest: surface tension forces [1, 2].

In terms of scaling laws, if the typical length of a structure is L , capillary forces are proportional to L , while pressure forces (such as wind drag) or elastic forces are proportional to L^2 and body forces (such as gravity) to L^3 . When all the dimensions of a given structure are scaled down, capillary forces decrease slower than pressure and body forces and eventually become dominant. As a consequence, a liquid droplet smaller than the 'capillary length', $L_c = \sqrt{\gamma/\rho g}$, where γ and ρ are respectively the surface tension and the density of the liquid, adopts a spherical shape when deposited

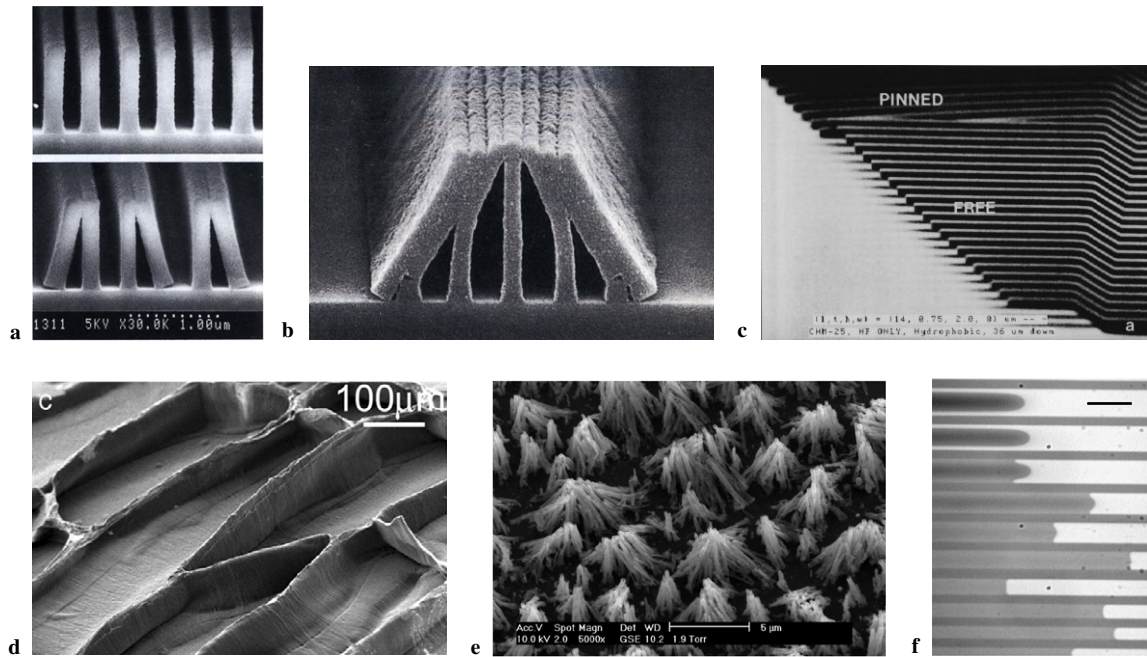


Figure 1. (a) A micropattern in photoresist (bottom) fatally collapses after being rinsed by pure water but stands unaffected (top) if a liquid of low surface tension is used. (b) ‘Tepee’ structures obtained as many lamellae stick together, pictures reprinted from [9], with permission of Japan Society of Applied Physics. (c) Stiction of micromachined cantilever beams as their lengths exceeds a critical limit, picture reprinted with permission from reference [4] (©1993 IEEE). (d) and (e) Collapse of carbon nanotubes ‘carpets’ when put in contact with a liquid and dried: cellular structures or bundles are formed depending on the characteristics of the carpets, pictures reprinted from [18] with permission of PNAS and from [17] (©2003 American Chemical Society), respectively. (f) Collapse of the walls of soft microfluidics channels as their width exceeds a critical limit (the liquid in dark flows from left to right; the channels have collapsed in the upper images), image reprinted from [31] with permission of Elsevier.

on a surface. Beyond prescribing the shape of liquid droplets, may capillary forces deform a solid structure? The aim of the present review is to address this question.

Everyday experience teaches us that wet hairs—a flexible solid structure in contact with a liquid interface—assemble into bundles. However, beyond cosmetics applications, the effect of capillary forces is crucial in micro- and nanotechnologies. Indeed, most of the techniques used to build micro-electromechanical systems (MEMS) rely on wet lithography: a layer of photosensitive resin is selectively etched into a given microstructure and the removed material is rinsed away in a solvent [3]. As the structure is dried, capillary bridges may attract, deform, stick or even break flexible parts (figures 1(a)–(c)). This ‘stiction’ phenomenon is a strong limiting factor in the design of microstructures involving cantilever beams [4–8], slender walls [9, 10] or microcontact printing stamps [11, 12]. More generally, stiction issues in micro-machining have been widely reviewed in the literature [13–15]. Similarly, arrays of micro- or nanorods tend to form bundles in wet conditions. Cellular or ‘tepee’ structures have indeed been observed with ‘carpets’ of carbon nanotubes [16–20], ZnO or Si nanowires [21–23], polymeric micro-pillars [24–26] (figures 1(d) and (e)) or even possibly with hairy plant leaves with debated impact on surface wetting properties [27–29]. Surface tension may finally induce the collapse of microchannels (figure 1(f)) covered with thin walls in soft lab-on-a-chip systems [30–33] or possibly the collapse

of hollow carbon nanotubes partially filled with liquid [34]. Deformations of slender structures by capillary forces are, however, not limited to engineering issues but are also involved in biological systems such as the flexible legs of water striders [35, 36], insect tarsi [37] or the plastron of aquatic insects [38, 39]. More dramatically, capillarity can cause the collapse of lung airways of premature infants with fatal consequences [40–44].

Although the same physical ingredients (surface tension, elasticity) are present in all these very different fields ranging from microtechnologies to biological systems, they are usually studied independently. The aim of this review is to provide a general framework of the interplay between surface forces and elasticity through a sequence—non-exhaustive—of model experiments that have been recently carried out. We first describe the minute deformation induced by a liquid droplet on a bulk surface, then focus on large amplitude deformations of slender objects and define a characteristic length scale, the elasto-capillary length, present in any problem combining bending stiffness and surface forces. In section 3 we review the problem of stiction (as in ‘wet hair’ issues), while section 4 describes how a slender rod forced to pierce an interface may buckle. In section 5 we expand the interaction between bending and capillarity to flexible sheets and describe how a thin membrane may spontaneously wrap around a liquid droplet. We finally conclude with an opening to more complex problems where geometrical constraints induce stretching in addition to bending and surface forces.

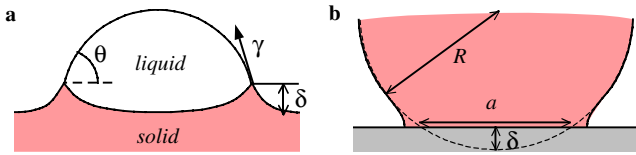


Figure 2. (a) Liquid droplet deposited on a soft substrate: the solid is deformed in the vicinity of the contact line (sketch adapted from [49]); (b) elastic sphere in contact with a solid surface, without any normal load: in the presence of surface forces (adhesion), the contact is not punctual but presents a disc shape of diameter a (sketch adapted from [55]).

2. Elasto-capillary length

In this section we define the characteristic length scales that quantify the relative importance of surface forces with respect to elastic rigidity. We first consider bulk elastic bodies and then focus on slender structures.

2.1. Capillarity and bulk elasticity

Consider a liquid droplet with surface tension γ deposited on an ideally smooth and uniform solid substrate. The liquid adopts a contact angle of value θ , which is classically set by a balance between surface forces at the contact line [2]. The balance of the horizontal components provides θ (Young’s relation). However, the vertical components are usually not considered, which is not totally correct as pointed out in the pioneering works from Lester and Rusanov [45, 46]. Indeed the finite vertical component $\gamma \sin \theta$ pulls on the substrate (figure 2(a)), thus deforming it¹. If δ is the typical amplitude of deformation of the pinched region, the corresponding force is of the order of $E\delta$ per unit length, where E is the Young’s modulus of the substrate, which leads to [47]

$$\delta \sim \frac{\gamma}{E} \sin \theta. \quad (1)$$

In the typical case of water ($\gamma \sim 70 \text{ mN m}^{-1}$) on glass ($E \sim 70 \text{ GPa}$), the ratio γ/E is of the order of 1 pm (10^{-12} m) and is not accessible. However, micron-size rims are observed at the vicinity of contact lines on rubbery solids ($E \sim 100 \text{ kPa}$) and have successfully been interpreted as a consequence of surface tension forces [48–51] (figure 2(b)). These deformations are found to result in contact angle hysteresis [52], in visco-elastic dissipation induced by a moving contact line [47, 53] and in enhanced nucleation density in condensation processes [54].

The deformation of bulk solid induced by surface energy may nevertheless be amplified by geometry. For instance, if an elastic sphere is put in contact with a solid surface (figure 2(b)), a compression of the sphere by a minute quantity δ results in a contact zone of extension $a \sim \sqrt{\delta R}$, which corresponds to an amplification of δ by a quantity $\sqrt{R/\delta}$. If the surface is adhesive, extending the contact area decreases the surface

¹ Note that the Laplace pressure inside the droplet results in a vertical downward force given by $\pi r^2 \frac{2\gamma}{R}$, where R is the radius of curvature of the droplet and r its perimeter ($r = R \sin \theta$). This force exactly compensates the upwards vertical component of the capillary force at the contact line $2\pi r \gamma \sin \theta$: the total force on the substrate is zero.

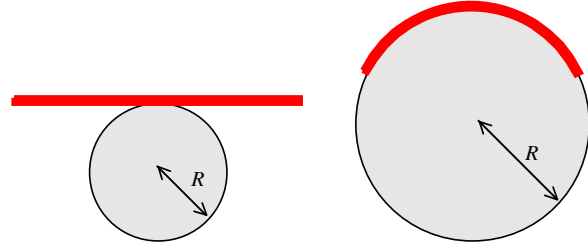


Figure 3. An illustration of the elasto-capillary length L_{EC} : a flexible sheet is put in contact with a cylinder of radius R coated with a wetting liquid. The sheet spontaneously wraps the cylinder if $R > L_{EC}/2$.

energy of the system by a quantity of the order of γa^2 , where γ represents the work of adhesion². In their milestone work on adhesion Johnson *et al* have estimated from an extension of Hertz theory the corresponding elastic energy $Ea^3(\delta/a)^2$ [55]. Balancing both terms finally leads to the extension of the contact zone:

$$a \sim \left(\frac{\gamma}{E} R^2 \right)^{1/3}, \quad (2)$$

which involves the same length scale γ/E and provides a benchmark for measuring the adhesive properties of materials.

In conclusion, the ratio γ/E gives the length scale for deformations of bulk elastic solids induced by surface forces. This length scale ranges from atomic scale (usual solids) to microns (elastomers). We focus now on the deformation of slender structures, which can be much more compliant.

2.2. Slender structures: elasto-capillary length

Consider an elastic plate of length L , width w and thickness h , coated with a thin layer of liquid of surface tension γ that is put in contact with a rigid cylinder of radius R also coated with the same liquid (figure 3). Wrapping the cylinder with the plate would result in a gain in surface energy of $2\gamma wL$, but in an increase of elastic energy of $BwL/2R^2$, where B is the bending modulus of the thin plate, $B = Eh^3/12(1 - \nu^2)$, E and ν being the Young’s modulus and Poisson ratio of the material, respectively [56, 57]. The plate is thus expected to spontaneously wrap around the cylinder if $R > \sqrt{B/\gamma}/2$ ³. We define as elasto-capillary length the characteristic length scale:

$$L_{EC} = \sqrt{\frac{B}{\gamma}} \sim \sqrt{\frac{Eh^3}{\gamma}}, \quad (3)$$

which thus compares bending stiffness and surface tension. As described in this simple example L_{EC} sets the typical curvature that capillary forces can induce on a flexible sheet: a structure is significantly deformed by surface tension if its length is large in comparison with L_{EC} . Indeed capillary forces produce a larger torque (larger lever arm) on a larger structure. If a given

² The work of adhesion is formally equivalent to the surface tension of the liquid presented in the first example.

³ In practice the sheet develops a finite contact zone even in the case $R < \sqrt{B/\gamma}/2$ and slightly bends over the rod because of the finite thickness of the liquid coating.

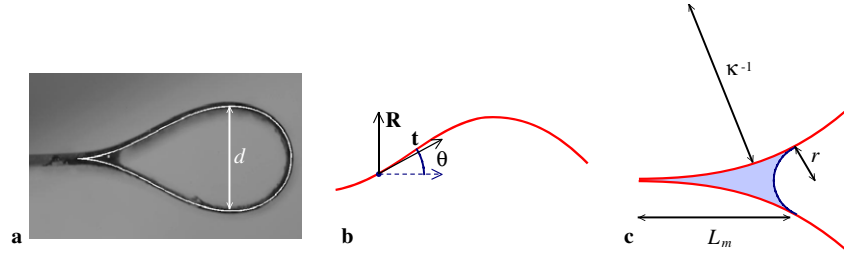


Figure 4. (a) Racket shape obtained as a strip sticks on itself (white line: calculated profile). L_{EC} sets the length scales of the shape (in particular $d = 0.89L_{EC}$), image credit Doppler and Py [58]. (b) Variables used in Euler’s elastica equation (equation (4)). (c) Zoom into the liquid meniscus to illustrate the boundary conditions in elasto-capillary problems. The initial curvature κ is proportional to L_{EC} .

structure is scaled down uniformly by a factor $\lambda < 1$, L_{EC} is multiplied by a factor $\lambda^{3/2}$ ($L_{EC} \propto h^{3/2}$) and thus decreases faster than the length of the structure. Capillary forces are effectively crucial for smaller structures since the condition $L \sim L_{EC}$ may eventually be reached, which is the case in the different examples reviewed in section 1.

Measuring L_{EC} by wrapping cylinders of various radii is, however, not very practical. It is easier to observe the equilibrium state obtained when the free ends of an elastic strip coated with a liquid layer are brought in contact together [58]. If the strip is long enough, the contact zone zips up and forms a racket shape (figure 4(a)), which can also be found with carbon nanotubes [59, 60], models for graphene sheets [61] and in biological filaments [59] sticking onto themselves. The shape of the racket is given by a balance between the zipping action of surface tension (in order to decrease the liquid/air area) and the bending energy which increases as the radius of the racket is reduced. Since this shape does not depend on the total length of the strip (provided that the strip is long enough), all its dimensions are proportional to the single length scale left in the problem, L_{EC} . We found it convenient to measure the width of the racket d (figure 4(a)) and use the numerical relation: $d = 0.89L_{EC}^4$. We describe in the following section how the numerical prefactor can be estimated.

2.3. Adhesion boundary conditions in elasto-capillary problems

The equilibrium shape of the racket is obtained by solving the classical Euler elastica equation for a beam of bending stiffness B [57]:

$$B \frac{d^2\theta}{ds^2} \mathbf{e}_z + \mathbf{t} \times \mathbf{R} = \mathbf{0}, \quad (4)$$

where θ is the angle made by the tangent to the lamella \mathbf{t} with the horizontal at the curvilinear coordinate s (see figure 4(b)), \mathbf{e}_z the vector perpendicular to the plane and \mathbf{R} the constant vectorial tension of the beam (in the present case, \mathbf{R} only has a vertical component). The *elastica* equation can be solved numerically once the relevant boundary conditions are defined. Most of these conditions are trivial (initial and final values for θ , position of one end). However, within the limit of

⁴ This result is different from [60] where the linear equation for small deflection was used beyond its range of validity.

vanishing menisci, the interplay between capillary forces and elasticity results in an interesting boundary condition for the curvature of the beam at the contact point: the curvature $\kappa = d\theta/ds = \sqrt{2}/L_{EC}$ [62]. Similar boundary conditions appear in all elasto-capillary problems (though with a prefactor depending on the actual configuration of the contact), and more generally in all situations where a flexible strip is in contact with an adhesive surface (e.g. spontaneous peeling of thin films [63]), delaminates [64, 65] or is cleaved [66, 67].

A general variational derivation of this curvature jump is subtle [68, 69] but we give here a simple argument based on the forces due to the meniscus (for a detailed derivation of these forces see [70]). If the volume of the meniscus is small enough, the radius of curvature of the meniscus is given by $r \sim \kappa L_m^2$, where L_m is the length of the meniscus and κ the average curvature of the strip in the meniscus region (figure 4(c)). Laplace’s law sets the relative pressure inside the liquid: $P = -\gamma/r$. The total pressure force $\gamma/\kappa L_m$ diverges as the meniscus vanishes. However, the resulting torque per unit width remains constant, $PL_m^2 \sim \gamma\kappa^{-1}$. The resulting radius of curvature of the lamella with a bending rigidity B is thus independent of the volume of the meniscus:

$$\kappa^{-1} \sim \sqrt{\frac{B}{\gamma}} = L_{EC}. \quad (5)$$

The actual prefactor depends on the configuration: $\kappa^{-1} = L_{EC}/\sqrt{2}$ for the ‘racket’ (a strip sticking on itself) and $\kappa^{-1} = L_{EC}/2$ for the common case of a strip sticking onto a rigid substrate (curved or not).

This boundary condition on the curvature is finally illustrated in figure 5 where a thin strip is bent into a loop and deposited at the surface of a liquid. As the strip can slide on the liquid, neither horizontal forces are acting on the strip, nor vertical forces for symmetry reasons (we neglect here the weight of the strip). A simple torque is thus only applied at both ends, and the loop takes a circular shape. In this simple configuration, equation (5) can be easily inferred from energy minimization. If the loop is tightened by dx , wet solid replaces dry solid and some liquid/air interface is suppressed. This leads to a difference in surface energy (per unit width): $(\gamma_{SL} - \gamma_{SV} - \gamma_{LV})dx = -\gamma(1 + \cos\theta)dx$, where θ is the contact angle of the liquid on the surface. Length conservation gives $dx = -2\pi dR$, which results in a increase in bending

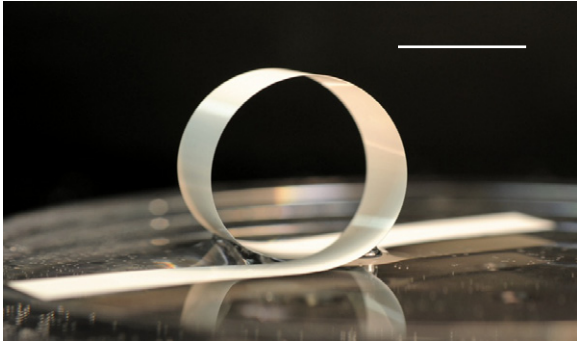


Figure 5. Lamella forming a loop at a liquid interface, the radius R of the circular loop given by $R = L_{EC}/\sqrt{2(1 + \cos \theta)}$, where θ is the liquid contact angle on the stripe (scale bar: 3 cm).

energy $\frac{1}{2} \frac{B}{R^2} dx$. At equilibrium the radius of the circle is thus given by

$$R = \frac{1}{\sqrt{2(1 + \cos \theta)}} L_{EC}.$$

Again we find a curvature jump proportional to $1/L_{EC}$. In principle one could measure the elasto-capillary length L_{EC} from the radius of the circle. But in practice, this method can only be used if R is larger than the meniscus size ($L_{EC} \gg L_c$), but still smaller than the size above which the structure is deflected by its own weight.

In the different situations explored in this section L_{EC} was the sole length scale. We focus in the next section on ‘stiction’ problems where additional geometrical constraints are present.

3. Wet hairs

In most practical applications, slender microstructures are not free but clamped on a substrate, which leads to additional geometrical constraints. As presented in the introduction, many micro-devices involve cantilevers fixed at a narrow distance from a solid wall or arrays of lamellar or rod-like structures separated by a short gap (figure 1). Such structures tend to collapse irreversibly in wet environments under the action of capillary forces. The aim of the present section is to describe the conditions leading to the collapse of ‘hairy’ structures.

A nice example of the collapse of arrays of parallel lamellae can be found in ferns from temperate forests. Fern spores are stored in specific capsules, sporangia and are suddenly released as sporangia burst under dry weather conditions [71, 72]. Botanists have discovered that the shells of the capsules are covered with parallel platelets reminiscent of micron-size ribs. The spacing between the platelets is initially filled with water, which does not lead to any interaction. However, the evaporation of water induces capillary forces, which result in local torques on the shell. This principle has been recently used to produce biomimetic micro-actuators sensitive to humidity (figure 6(a)) [73]. In this situation, the lamellae are short and rigid, and clamped on a flexible base. However, a variety of practical applications involve

the opposite configuration (long lamellae clamped on a rigid substrate), which we explore now.

As a simple example of ‘wet hair’, we consider the situation where two vertical parallel plates separated by a distance d are brought into contact with a bath of wetting liquid (figure 6(b)). In the classical case of rigid plates, the liquid rises up to an equilibrium height where capillary forces are balanced by the weight of the liquid column: $h_J = 2\gamma/\rho g d$ (Jurin’s law [2]). However, if the plates are flexible and clamped along their upper edge, the depression within the rising liquid brings the plates closer, which in turns favors a higher capillary rise [70]. When the plates are long enough, a contact zone zips up to a distance L_{stick} from the clamps (figure 6(c)). In the zipped part the lamellae are in contact and the actual thickness of interstitial liquid is of the order of surface roughness. If the meniscus formed by the liquid is small enough, gravity can be neglected and the adhesion of the lamellae by the liquid is only limited by the bending energy, which increases as the zipping front approaches the clamps. In this regime, the sticking distance is independent of the total length of the lamellae and follows the law [74, 70, 75, 76]

$$L_{stick}^4 = 9d^2 L_{EC}^2/2, \quad (6)$$

(provided $d \ll L_{stick}$). In practice, a structure length lower than L_{stick} avoids stiction issues. Additional ‘tricks’ may also be used such as vanishing surface tension forces under supercritical phase transitions [15, 77] or flash release [78], or as strengthening of the hairs by electric fields [79].

In terms of scaling, the typical curvature of the lamellae is of the order of $\kappa \sim d/L_{stick}^2$, leading to the bending energy per unit width $B(d/L_{stick}^2)^2 L_{stick}$. The balance between bending and surface energies γL_{stick} finally gives $L_{stick} \sim d^{1/2} L_{EC}^{1/2}$. In agreement with the sticking boundary condition (equation (5)), we find $\kappa \sim 1/L_{EC}$. As already pointed out [80], this description is similar to the classical cleavage fracture by Obreimoff [66], where a thin layer of mica is split by pushing a blade of thickness d towards the crack front (figure 6(d)). A measurement of the length L_{crack} , separating the front from the blade, provides a measure of the fracture energy of the material, which plays the role of the liquid surface tension in this problem [67].

The same scaling finally gives the extension λ of a blister obtained when a thin layer deposited on a soft adhesive substrate is uniaxially compressed by a distance ΔL (figure 6(e)). In the case of blisters of small amplitude d , a geometrical relation gives $d^2 \sim \lambda \Delta L$, which combined with the relation for wet hair $\lambda \sim d^{1/2} L_{EC}^{1/2}$, leads to [64, 65, 81]

$$\lambda \sim \Delta L^{1/3} L_{EC}^{2/3}. \quad (7)$$

The blister size, λ does not depend on the mechanical properties of the uniaxially compressed substrate. However, the critical compression leading to the formation of blisters depends on the Young’s modulus of the substrate [65]⁵. We expect this simple scaling to be relevant to experiments

⁵ Note that this relation is not valid for a rigid substrate where the combination of mixed fracture modes selects the extension of the blisters [82].

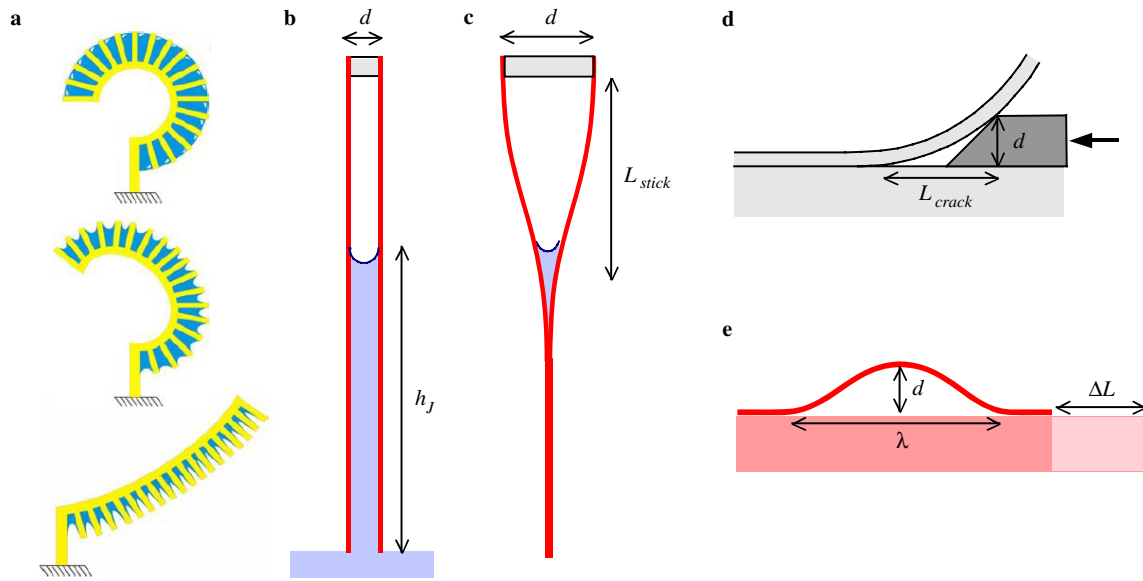


Figure 6. (a) Actuation of rib-like structures as the liquid filling the inter-spacing evaporates (image reprinted from [73], with permission from IOP). (b) Classical capillary rise between rigid plates separated by a narrow gap d . (c) Sticking length for two long flexible plates clamped at a fixed distance. (d) Analogy with crack length in cleavage, sketch adapted from [66]. (e) One-dimensional blister formed as a thin film adhering on a soft substrate is uniaxially compressed.

involving the release and bond back of prestressed thin films that also lead to regularly spaced blisters [83, 84].

Coming back to the problem of wet hair, bundles are observed when a brush of long lamellae is progressively removed from a liquid bath (figure 7(a)). The formation of these bundles relies on a cascade of adhesion of pairs of sub-bundles, which leads to a hierarchical pattern. Large bundles of size N are formed as pairs of smaller ones, of size $N/2$ on the average, merge at a distance $L_{stick}(N)$ from the base of the brush. These bundles are $N/2$ times more rigid than a unit lamella (the interstitial liquid promotes the relative sliding of lamellae) and their effective separating distance is $Nd/2$. By extending the adhesion law for a pair, we find the sticking distance of a bundle composed of N lamellae:

$$L_{stick}(N) = (N/2)^{3/4} L_2. \quad (8)$$

This formula sets the maximum size N_{max} for a bundle in a brush of lamellae with length L . However, smaller bundles are also present if the sticking distance of neighboring bundles exceeds L , which leads to a broad size distribution. The range of this distribution ($0.3N_{max} < N < N_{max}$) can finally be predicted through a statistical description of the aggregation process [85].

From a practical point of view, most applications do not involve 1D arrays of lamellae, but rather carpets of flexible bristles (carbon nanotubes, Si or polymeric nanorods). Although rod-like structures bring an additional length scale, the radius r of the rod, the physical description of stiction is very similar to lamellae. The thickness of the lamellae h is basically replaced by r , since the bending stiffness $B_{rod} = \pi E r^4 / 4$ is compared with the capillary force γr in the formula for L_{EC} [87]. However, the coalescence into growing bundles follows a different scaling law $L_{stick}(N) \sim N^{3/8} L_2$ due to the

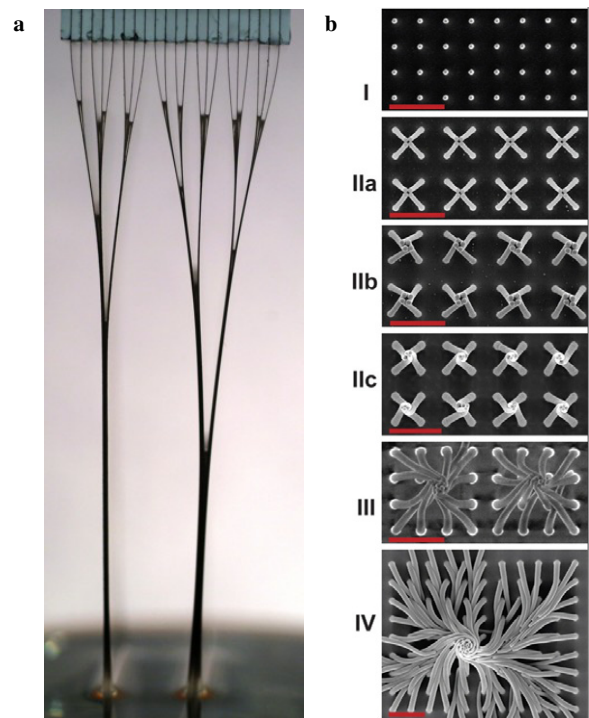


Figure 7. (a) Bundles formed as a brush of flexible lamellae is removed from a bath of wetting liquid (brush width 2 cm). Image reprinted from [74]. (b) Bundling of polymeric arrays of nanorods initially immersed in a volatile solvent: longer bristles lead to larger clusters and even tend to form helical structures (scale bars $4 \mu\text{m}$, images reprinted from [86] with permission).

2D lattice for the rods (the number of close neighbors is larger than in the 1D case) [62]. Finite size effects may also play an important role in the coalescence process as comprehensively

discussed in a very recent review on the stability of height aspect ratio micro-pillar arrays [88].

In the case of soft rods (e.g. made of polydimethylsiloxane, PDMS) the contact area between adhered pillars depends on the adhesion energy and can be described with JKR theory (equation (2)) that can be adapted to cylindrical geometries [89]. As the rods are in contact the adhesion energy between a pair of rods of radius r and length L is of the order of $\gamma(\gamma/E)^{1/3}r^{2/3}L$, which leads to a modified elasto-capillary length, $L_{ECJKR} \sim (Er^3/\gamma)^{1/2}(Er/\gamma)^{1/6}$. The relevance of this length scale has been experimentally validated with arrays of PMDS micro-pillars [90]. From a biomimetic engineering point of view, self-adhesion of micro-rods is also considered as a limitation to the development of universal adhesives inspired by gecko feet and based on van der Waals forces [91]. However actual seta of gecko feet present hierarchical structures reminiscent of bundles of wet hair [92], which would promote a strong adhesion to any rough surface, while avoiding fatal self-adhesion [93].

Long and flexible rods may finally develop intriguing helical bundles (figure 7(b)) that can be used as traps for nano-objects, as nicely demonstrated in experiments by Pokroy *et al* [86]. In this case, we believe that friction plays a crucial role in the process, forcing the bristles to follow an initial misalignment.

In this section we focused on lateral capillary forces between flexible slender structures. Nevertheless if such structures are initially immersed in a liquid, their extremities are eventually brought to pierce the liquid interface as the liquid evaporates, which lead to axial forces. We describe in the following section the possible buckling induced by this compressive load.

4. Piercing hairs

Water striders are famous for relying on surface tension to stand on water. Penetrating the water surface with their hydrophobic legs indeed requires a force equal to the perimeter of the leg times the water surface tension [94]. In the opposite situation of a carbon nanotube ‘forest’ initially immersed in a volatile solvent and then dried, compressive capillary forces arise as the end of the tubes start piercing the liquid interface (figure 8). Upon this compressive load the nanotubes may buckle and eventually collapse on the substrate [18]. Similarly, carbon nanotubes trapped in microbubbles or tubulin rods grown inside vesicles may also buckle if their length exceeds the diameter of their container [59]. Buckling occurs when the compressive force exceeds Euler’s critical load $(\pi/2)^2 B_{rod}/L^2$, where L and $B_{rod} \sim Er^4$ are the length and the bending stiffness of the micro-rods, respectively, r being the radius of the rod. Since the capillary force is given by $2\pi r\gamma$, we find that the rod buckles if it is longer than a critical length proportional to the elasto-capillary length:

$$L_{crit} = \frac{1}{2\sqrt{\pi}} \sqrt{\frac{B_{rod}}{\gamma r}} \sim 0.3 L_{EC}. \quad (9)$$

As the rod buckles the capillary force is amplified by a factor $1/\cos\alpha$, where α is the angle made by the end of the rod

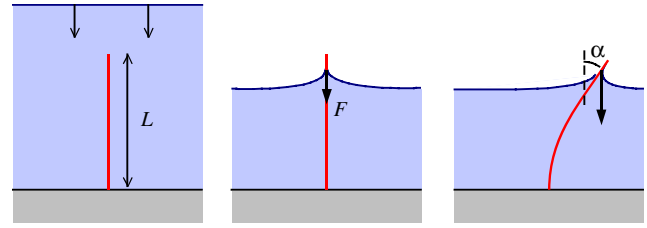


Figure 8. Piercing an interface with a flexible rod: if the capillary force $2\pi r\gamma$ is larger than Euler’s critical load $(\pi/2)^2 B_{rod}/L^2$ the rod buckles. The phenomenon is highly nonlinear since tilting the free end of the rod by an angle α results in a force increased by a factor $1/\cos\alpha$.

with the vertical (figure 8). This nonlinear behavior leads to complex post-buckling configurations, involving multistable states [95]. A similar phenomenon has been observed when a flexible ribbon is withdrawn from a bath of wetting liquid: the ribbon spontaneously buckles into high-order folding modes to reduce its width down to the spatial extension of the meniscus [96].

In the case of arrays, the rods may not only buckle under axial forces but also simultaneously form bundles as described in the previous section. As bundles are effectively stiffer than single rods, they are less prone to buckle and collapse. Depending on the lattice spacing, collaborative stiffening can lead to different final configurations such as ‘tepee’ or cellular structures [97].

Piercing watery films is also vital for filamentous fungi growing in moist environments. Indeed some species (such as *Schizophyllum commune*) have to produce surfactant molecules (hydrophobin) in order to grow aerial hyphae that allow dissemination of their spores [98]. Experimental evidence suggests these specific surfactants strongly increase the contact angle θ of water on hyphae wall: γ is replaced by $\gamma \cos\theta$, in equation (9), which decreases, or even suppresses, the critical load for buckling. Coming back to the case of aquatic insects, the maximum load that the leg can support increases with its length, but reaches a plateau when the length is of the order of L_{EC} [35, 36]. The measured length of actual water strider legs is apparently lower than L_{EC} , suggesting that the elasto-capillary length may play a role in natural selection.

Leaving aquatic insects, it has been suggested that aerial spiders also use the interaction between elasticity and capillarity to promote the damping properties of orb-webs [99]. Actual radial threads are longer than their apparent length and the authors argue that the excess length forms coils inside regularly spaced water beads observed along the thread. At a much lower scale, the coiling of a thread around a droplet is also reminiscent of the bead-on-string structures observed in nucleosomes, where DNA molecules wrap histone octamers, compacting the genetic material in our cells [100]. Non-compact DNA molecules would indeed not fit into nuclei whereas condensed DNA (like in virus capsids) would not allow complex gene expression and replication [101]. We consider now the simplified problem of an elastic filament in contact with a liquid droplet and derive the condition for the filament to spontaneously wind around the droplet (top inset

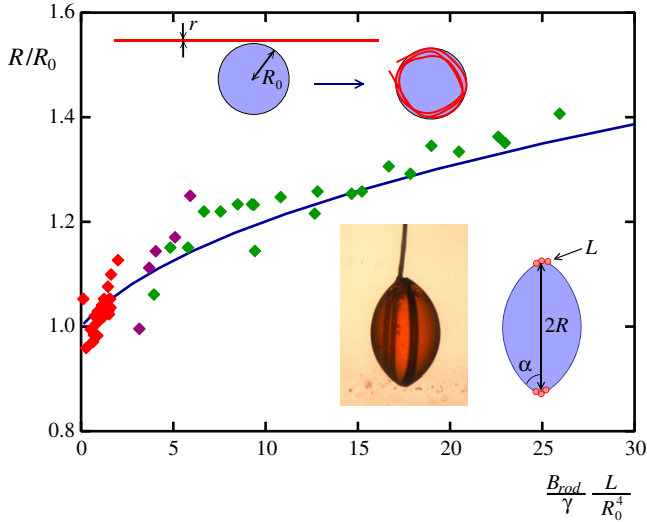


Figure 9. Liquid droplet maintained in levitation in a bath of matched density. A flexible thread put in contact with the droplet spontaneously winds around it if the radius R_0 of the droplet is large in comparison with L_{EC} . Depending on the number of loops the thread makes, the droplet adopts a lens shape characterized by an equator of radius R . Comparison of experimental measurements of R/R_0 as a function of the non-dimensional length of the thread (symbols) with the theoretical prediction from equation (10) (continuous line).

in figure 9). If a filament of length L , radius r and bending stiffness B_{rod} forms a coil around a liquid droplet of radius R_0 , the elastic energy stored in the coil corresponds to $\frac{1}{2} \frac{B_{rod}}{R_0^2} L$, while the gain in surface energy is $2\pi r \gamma L$. Spontaneous winding is then expected when $R_0 > L_{crit} \sim L_{EC}$.

In the case of spider webs, the typical radius of capture threads is of the order of $1 \mu\text{m}$ with a Young's modulus roughly estimated at 5 GPa (for relatively small deformations) [99], which leads to a bending stiffness B_{rod} of the order of $5 \times 10^{-18} \text{ N m}^2$. The corresponding elasto-capillary length $L_{EC} \sim 5 \mu\text{m}$ is therefore smaller than the size of the water beads observed on spider webs whose typical radius is $10 \mu\text{m}$, allowing coils to spontaneously form.

At a molecular scale, biophysicists have also developed models for the coiling of DNA around histones where DNA molecules are approximated by rods of bending rigidity $B_{rod} = \ell_p k_B T$, where $\ell_p \sim 50 \text{ nm}$ is the persistent length characterizing the thermal fluctuations of the macromolecule, and where the octamers are simplified as cylinders of radius $R_0 \sim 4 \text{ nm}$ [101]. The octamers provide 14 binding sites along a wrapping length of the order of 43 nm, with an adsorption energy that can be estimated as $6 k_B T$ per site [101], which leads to the equivalent elasto-capillary length $L_{EC} \sim 5 \text{ nm}$. The condition for spontaneous wrapping is thus verified.

However, wound droplets do not remain spherical, but take lenticular shapes with the elastic filament spinning along the equator (bottom inset in figure 9). The radius of the equator R is easily derived from the minimization of the global energy of the system $E = S\gamma + \frac{1}{2} \frac{B_{rod}}{R^2} L$, where S is the surface of the lens, with a constraint of constant volume, $\mathcal{V} = \frac{4}{3} \pi R_0^3$. The

minimum of energy corresponds to

$$\cos \alpha = \frac{1}{4\pi} \frac{B_{rod}}{\gamma} \frac{L}{R^4}, \quad (10)$$

where the angle α of the lens is geometrically related to R/R_0 by the volume constraint. This relation is in fairly good agreement with experiments carried out with centimeter size droplets suspended in a liquid bath of matched density (main plot in figure 9).

When the winding criterion is not satisfied, the rod is nevertheless slightly bent, as observed on micro-cantilevers [102, 103]. This effect should also allow us to drive a liquid droplet on a lamella with a gradient of stiffness, which may enhance the efficiency of biomimetic water-repellent surfaces [104].

5. Sheets and surface tension

Up to now we have documented the effect of surface tension on elastic rods (or two-dimensional plates) and shown that stiction is usually seen as a limiting factor in micro-fabrication. Conversely, we show in this section how surface tension provides a useful tool to build 3D microstructures by folding thin sheets with a liquid droplet. Capillary forces have, for instance, been used for the self-assembly of rigid micro-objects floating at a liquid interface [105]. Closer to the scope of this paper, the surface tension of molten solder droplets deposited at the hinges drawn on thin metallic sheets is capable of folding the panels of the templates into 3D microstructures. The structure is then frozen as the solder cools down [106, 107]. The principle of the folding relies on the minimization of the surface of the liquid in contact with air. Figure 10(a) illustrates the example of a micron-size cube obtained with this technique, but numerous shapes can be obtained with different templates [108–111], including elegant micro-boxes [112]. Submicron scales have even been recently reached with promising applications to nanotechnologies [113–115].

This technique is very interesting, since it provides a way to produce 3D microstructures, which is difficult with the conventional etching and layer deposition techniques derived from micro-electronics manufacturing that leads to quasi-planar objects.

One advantage of using hinges is the possibility to predict and control the final shape of the structures (in this case, the description of the folding does not involve elasticity). However, the micro-fabrication of predefined articulations remains a technological challenge and constitutes the major drawback of this technique. We therefore focus on situations where surface tension acts on plain elastic sheets. As a simple example, we consider the case of a water droplet deposited on a flexible triangle of side L , thickness h and bending stiffness $B \sim Eh^3$. If the triangle is flexible enough, it spontaneously wraps the drop (figure 10(b)), reducing the liquid–air area at the cost of elastic deformation of the sheet [58]. This is only possible if the gain in surface energy (of the order of γL^2) overcomes the elastic bending energy (of the order of B , if the sheet folds over its own size, i.e. if the radius of curvature



Figure 10. (a) Capillary ‘origami’. Closing of hinged structures inside a liquid droplet [107] (molten solder on metal templates). Copyright Wiley-VCH Verlag GmbH & Co. KGaA. Reproduced with permission. (b) and (c) Self-wrapping of a flexible sheet (PDMS and silicon) around a droplet of water leading to different 3D structures depending on the initial template, images reprinted from [58] and [116], respectively, with permission.

is of the order of L). In other words spontaneous wrapping occurs if the sheet is larger than a critical length L_{crit} , which is proportional to the elasto-capillary length L_{EC} . Figure 10(b) presents a series of pictures of an evaporating droplet of water deposited on a thin triangle made of polydimethylsiloxane (PDMS). As the liquid evaporates, a pyramid is progressively formed. The edges seal almost perfectly except in three corners, where evaporation still takes place. Below a certain volume, the structure starts to collapse and eventually reopens, leading to the same triangular template (see the movie in Electronic Physics Auxiliary Publication Service (EPAPS) in [58]). However, the 3D structure can be frozen at any time of the process if some cross-linking agent is added to the evaporating liquid, which may open a new way of producing micro-devices. Indeed the process will be all the more efficient as capillary forces become dominant when the sizes are scaled down. At molecular scales, direct numerical simulations even show that a graphene sheet should wrap a nanodroplet [117].

Depending on the geometry of the initial template, a variety of shapes can be obtained by this capillary origami technique, e.g. a quasi-sphere from a flower shape (figure 10(b)) or a cube from a cross-template [58]. However, predicting the final shape is not always straightforward: starting from a square pattern, the system seems to first fold all four corners towards the center, but finally selects

a cylindrical solution [118], as illustrated in the last column in figure 10(c). Although the value of the critical length for closing the structures is proportional to L_{EC} , the actual prefactor depends on the initial template: $L_{\text{crit}} \simeq 12L_{\text{EC}}$ for triangles and $L_{\text{crit}} \simeq 7L_{\text{EC}}$ for squares [58]. The exact description of capillary origami systems is, however, difficult since it requires the coupling of nonlinear equations for large amplitude folding of the sheet to the three-dimensional shape of the drop. For a given volume of liquid several equilibrium states may even coexist as shown by the theoretical study of a 2D version of the problem [58]. For instance, if the origami is formed after the impact of a droplet on an elastic template, the final shape may depend on the initial kinetic energy, as nicely demonstrated in [119]. Figure 11(a) illustrates different final shapes obtained as the velocity of the impacting droplet is increased.

As a practical example, 3D photovoltaic cells with enhanced efficiency were engineered through the spontaneous wrapping of wet beads by thin silicon films (figure 10(c)) [116]. The reopening of a closed origami structure can also be actuated by an electric field with a potential application to digital displays: the structure opens beyond a critical voltage U_{open} and closes back below a lower voltage U_{close} . Both critical voltages can be estimated from the size and the bending stiffness of the sheet and the surface tension of the liquid. These voltages are proportional to $\sqrt{\gamma h/\epsilon}$, a

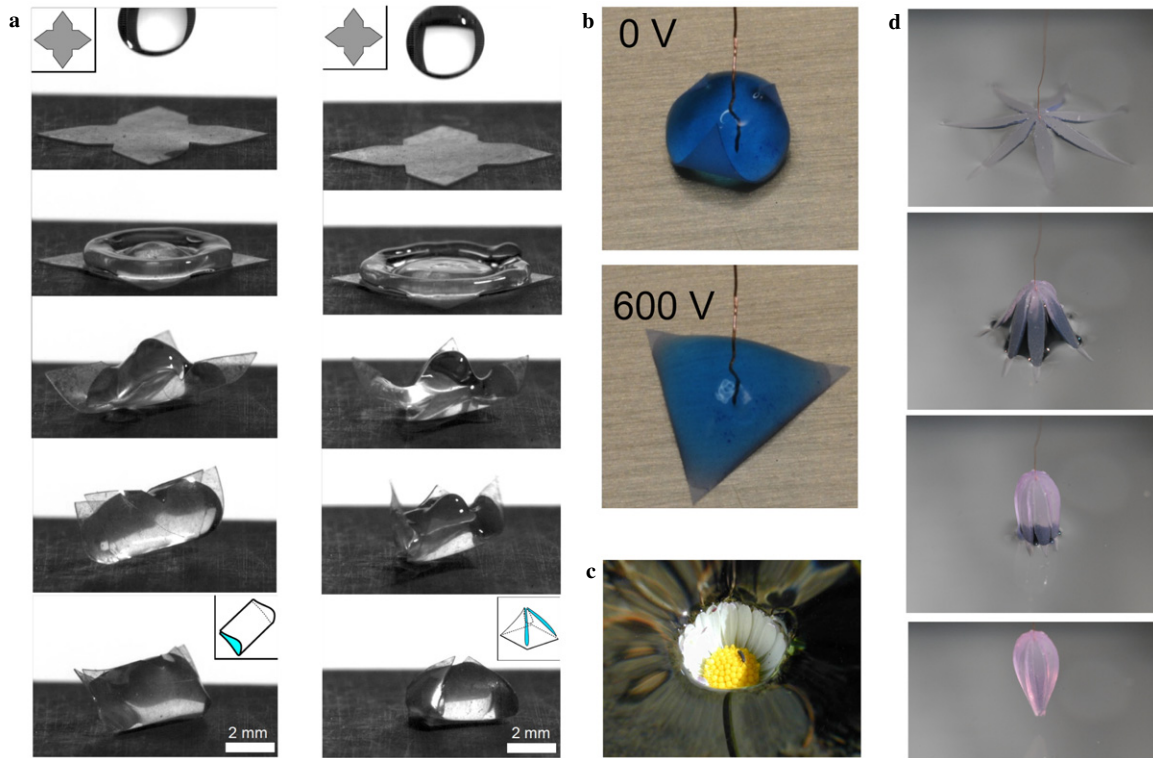


Figure 11. (a) Dynamical origami: different final shapes are obtained with the same template as the velocity of the impacting droplet is increased (image credit A Antkowiak [119]). (b) Reopening actuated by an electric field: a voltage is applied between the droplet and the substrate; beyond a critical value the structure reopens [120] (image credit Piñeira). (c) The corolla of a daisy closes as the flower is progressively submerged (licensed under the Creative Commons Attribution ShareAlike 3.0 License). (d) Elasto-pipette: a flower-shaped thin sheet is used to grab and deposit a defined quantity of liquid [121, 122] (image credit Hure).

voltage which compares capillary and electrostatic energies, ϵ being the dielectric constant of the sheet [120, 123].

In the botanical world, closing flowers can also be vital for aquatic plants that rely on wind or aerial insects for dissemination. The corollas of certain varieties of *Nymphaeoides* flowers, that usually float at the surface of ponds but are tethered to the ground by their stem, are found to close hermetically if they sink after a sudden increase of the water level [124] (figure 11). Trapping an air bubble inside the flower thus preserves the reproductive organs from flooding. Although capillary forces are not directly involved in the closing mechanism (which relies at that scale on a balance between bending elasticity and hydrostatic pressure), surface tension plays a crucial role in preventing water from penetrating into the flower through the spacing between the petals. Inspired by this botanical example, the opposite situation has been considered [121], where an elastic template imitating a corolla is brought in contact with the surface of a liquid (figure 11(d)): when pulled back, this ‘elasto-pipette’ spontaneously grabs a precise amount of liquid that can be redeposited on another surface [121, 122].

Interesting effects also occur when a membrane floating on an infinite bath of liquid is perturbed. Parallel wrinkles, for instance, are observed as a thin sheet of polymer floating on water is uniaxially compressed (figure 12(a)). Far from the edges, the large wavelength of the wrinkles is set by

a balance between the bending stiffness of the sheet and gravity (liquid weight): $\lambda \sim (Eh^3/\rho g)^{1/4}$ [125, 126]. However, the wavy edge of the sheet also deforms the liquid surface and capillary forces tend to decrease the amplitude and wavelength of the buckling mode. As a result, a cascade of wrinkles is observed, which goes from this wavelength to a much shorter one. The resulting cascade shape results from a balance between bending rigidity, surface tension and gravity, and therefore involves the elasto-capillary length L_{EC} as well as the capillary length $L_c = \sqrt{\gamma/\rho g}$ [126].

A different morphology of wrinkles is observed when a droplet (smaller than the capillary length L_c) is deposited on the same thin film floating on water as illustrated in figure 12 [127]. Indeed the surface tension of the droplet generates radial tension in the film, which leads to an orthoradial compression and eventually to radial wrinkles. In terms of scalings, the bending energy per unit width corresponding to wrinkles of wavelength λ and amplitude A developed over a typical length L is proportional to $B(A/\lambda^2)^2$, where $B \sim Eh^3$ is the bending stiffness of the film, while the tensile energy scales as $\sigma hL(A/L)^2$, where σ is the applied tensile stress. Balancing these two ingredients leads to a typical wavelength $\lambda \sim (B/\sigma h)^{1/4} L^{1/2}$ [128]. In the axisymmetric case of the droplet with radius a pulling on the sheet through capillary forces, the radial stress distribution is expected to follow $\sigma_{rr} \simeq$

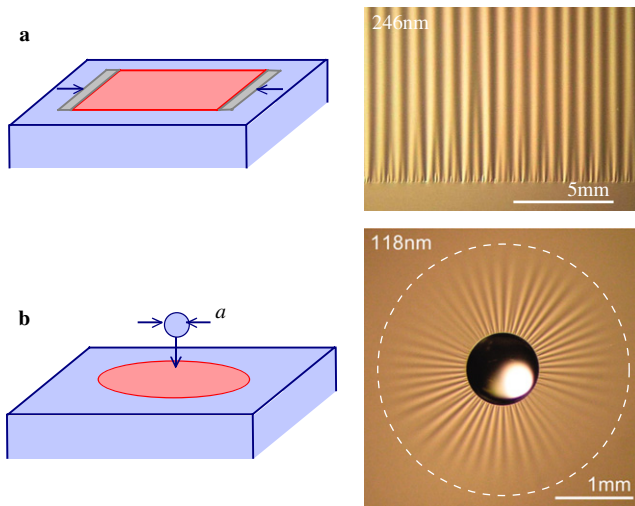


Figure 12. Experiments with thin polystyrene films deposited on water. (a) Uniaxial compression leading to a cascade of wrinkles perpendicular to the strain direction. The large wavelength wrinkles far from the edge result from a balance between gravity and bending stiffness while short wavelength wrinkles at the edges rely on surface tension forces [126]. Image credit Huang and Menon. (b) Water droplet of radius a deposited on a thin polystyrene film of thickness from 118 nm floating on water. The number of radial ridges then formed is given by $N \sim \sqrt{a/L_{EC}}$, while the extension of the ridges (white circle in the first image) is set by $\ell \sim a\sqrt{Eh/\gamma}$ as a result of a balance between surface tension and stretching energies. Picture reprinted from [127].

$\sigma_0(a/r)^2$ [57], with $\sigma_0 \sim \gamma/h$. The number N of wrinkles is independent of the radial coordinate r , which leads to a local wavelength $\lambda \sim r/N$. Taking a typical length scale $L \sim r$ and a wavelength $\lambda \sim r/N$ finally gives the number of wrinkles raying around the droplet:

$$N \sim (a L_{EC})^{1/2}. \quad (11)$$

Counting these wrinkles thus provides a measure of the bending stiffness of the thin polymeric membrane [127]. Note that local stresses and deformations have been more rigorously derived with the aim of determining the apparent contact angle of the liquid droplet on the plate [129–131]. However, these studies are limited to minute axisymmetric deformations without radial wrinkles, as has been experimentally observed with liquid Pb microdroplets deposited on graphite thin sheets [132]. In the case of polymeric films, the wrinkles are also found to damp out at a characteristic distance ℓ from the droplet as a result of the stretching of the membrane. Although analytical arguments to define this damping length have been missing until recently, ℓ has been empirically found to follow

$$\ell \sim a(\gamma/Eh)^{-1/2}. \quad (12)$$

In this expression we recognize the length scale γ/E , which characterizes bulk elastic. This length scale is expected to appear whenever surface tension leads to stretching. The non-dimensional number γ/Eh compares the stretching stiffness Eh with surface tension, and thus gives an estimate of the typical in-plane strains produced by the capillary force directly

pulling on a thin sheet. In a more general case of a liquid bath of surface tension γ^* different from the value γ for the droplet, very recent improvements in the theoretical description of the damping length scale have shown that the ratio ℓ/a should be a function of the non-dimensional parameter $\frac{Eh \sin \theta_0}{\gamma} \left(\frac{\gamma}{\gamma^*}\right)^3$, in agreement with experimental results where surfactant molecules have been added to the water bath [133].

More generally, surface tension forces may stretch a thin sheet without obviously pulling on it if the sheet is bent into a non-developable shape. For the same reason that it is impossible to draw a flat map of the Earth without distorting distances, folding a sheet in 3D requires, in most cases, some stretching. In geometrical terms, Gauss demonstrated in his *theorema egregium* that isometric transformations are only possible when the Gaussian curvature (product of the main curvatures) is preserved [134]. Smooth developable surfaces obtained by simply folding an initially flat sheet are therefore limited to generalized cones and cylinders. Producing shapes with non-zero Gaussian curvature thus relies on stretching energy as demonstrated by Alben and Brenner [135] in the context of ‘origami’ structures maintained by magnetic forces [136]. Similarly, fixing an initially flat sticker on a spherical shape requires stretching. The non-dimensional number Eh/γ thus controls the maximum size above which blisters are formed on the adhesive tape [137]. Adding stretching energy in addition to bending and surface tension energies opens a new axis (a new characteristic length scale γ/E) in the description of elasto-capillary problems.

6. Conclusion and perspectives

Surface tension forces play in general a negligible role at large scales, but they may induce dramatic effects when sub-millimetric sizes or very flexible objects are considered. We have reviewed many examples which are all described by the elasto-capillary length $L_{EC} = \sqrt{B/\gamma} \sim \sqrt{Eh^3/\gamma}$ characterizing the balance between bending and capillary forces: a structure with a size L larger than L_{EC} will be strongly deflected by surface tension forces. We see that, for a fixed thickness, large structures will eventually be deformed by capillary forces. At human scales this is not usually observed because gravity becomes dominant for scales above a few millimeters. However, elasto-capillary effects can be observed at macroscopic scales if the liquid weight is suppressed: an origami structure (a few centimeters wide) is created when a soap bubble is laid on a wet film (figure 13).

When all the dimensions of a structure (including thickness) are scaled down, we see that $L_{EC} \sim L^{3/2}$ decreases faster than the size of the structure, so that surface forces will eventually overcome elasticity. As recent years have witnessed a rapidly growing interest in micro- and nanostructures, we expect the study of the capillary effect on solids to take a more important part in engineering, and therefore in fundamental science. We finally observe that two types of problems have hardly been considered and should bear attention in the near future: dynamics and crumpling.

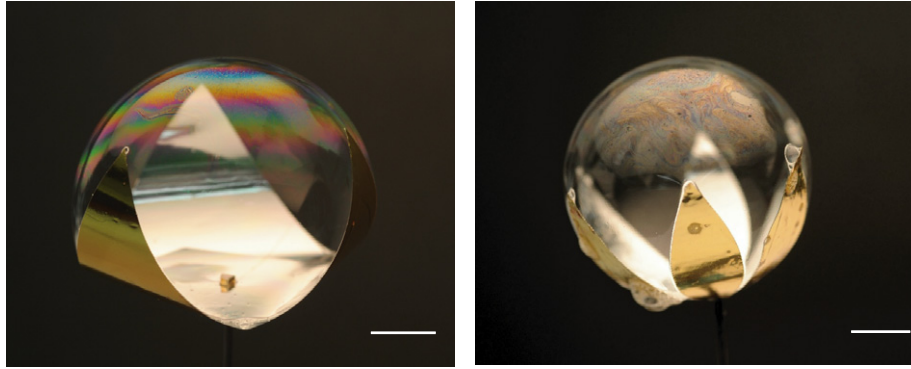


Figure 13. Capillary origami with soap bubbles: the shape of the bubble remains unaffected by gravity, which allows large scale experiments. Left image, triangular template; right image flower template (scale bar: 2 cm).

Except in a few cases, studies on elasto-capillary systems have been restricted to equilibrium situations. However, some capillary effects are essentially dynamical, such as spore ejection in basidiomycete fungi [138]. In the case of capillary origami, dynamics may affect the selection of the final rest configuration in the case of multiple equilibrium [119]. The determination of the time to reach equilibrium in elasto-capillary systems is of fundamental and practical interest. The dynamics of imbibition of strongly deformable media is currently studied through model experiments [139–141] in connection with industrial processes [142] or physiological issues (lung collapse).

Another interesting area for research is the case of very thin sheets more prone to crumpling than to smooth deformations. Indeed since the stretching modulus is proportional to the film thickness h while the bending modulus scales as h^3 , stretching a sheet becomes comparatively more difficult as thinner sheets are considered. Nevertheless, most boundary conditions are not, in general, compatible with a smooth developable surface and they induce the formation of singularities. In actual materials these singularities are regularized by some localized extension [143–145]. As a common example, crumpling a piece of paper induces concentrated marks along lines where the stretching energy is focused. These singular regions are usually deformed plastically and the marks do not vanish as the crumpled sheet is unfolded. We believe that surface tension forces may also lead to some energy focusing and crumpling. In such cases, we expect the length scale γ/E to play a role in the determination of the stability of very slender microstructures.

Acknowledgments

This review would have not been possible without the help of junior students and co-workers. We also thank numerous colleagues for their motivating encouragement and input:

- Students: L Moulin, S Réau, B de Gaudemaris, J Guilet, R Bastien, L Doppler, A Delbos, F Closa, A Calvar, A Bohé, D Salfati, G Batot, K Armoogum, F Chiodi, J Marthelot, T Cambau, L Bonnemay.

- Co-workers: A Boudaoud, C Py, C Baroud, S Neukirch, P Reis, D Vella (who provided numerous corrections to the manuscript), M Piñeirua, J Hure, Y Aoyanagi, A Takei, E Reyssat.
- Colleagues (non-exhaustive list): T Witten, H A Stone, E de Langre, N Menon, J van Honschoten, J W M Bush, M Fermigier, A Antkowiak, D Bartolo, B Audoly.
- We are finally very grateful to the different funding programs that allowed our junior team to grow up and develop: Société des Amis de l'ESPCI, ANR MecaWet, BQR ESPCI and BQR UPMC.

Appendix

We summarize in this appendix the characteristic length scales that can be relevant as additional forces may also interact with elasticity and surface energy. Comparing the size of an actual system with these different length scales should help to sort out the relevant physical ingredients presented in table A.1. In table A.2 the two competing effects are displayed in the first columns. If the size of the system is large in comparison with the corresponding length scale, the effect of the first column dominates the second one.

Table A.1. Symbols for the different physical parameters.

γ	Surface energy
E	Elastic Young's modulus
ν	Poisson ratio
L	Length of the structure
h	Thickness, for planar structures
r	Radius, for rod structures
$B = Eh^3/12(1 - \nu^2)$	Bending stiffness, for planar structures
$B_{\text{rod}} = \pi Er^4/4$	Bending stiffness, for rod structures
g	Gravity constant
ρ_l	Liquid density
ρ_s	Solid density
ω	Oscillation frequency (for flagella)
$k_B T$	Thermal energy

Table A.2. Characteristic length scales comparing pairs of competing effects: if the size of the system is large in comparison with the corresponding length scale, the effect of the first column dominates the second one. h and r correspond to the thickness and the radius of the structures for lamella or rod structures, respectively.

Effect 1	Effect 2	Length scale	Reference
Stretching rigidity	Surface energy	γ/E	[47, 55]
Surface energy	Bending rigidity	$\sqrt{Eh^3/\gamma}$ or $\sqrt{Er^3/\gamma}$	[59]
Gravity	Surface tension	$\sqrt{\gamma/\rho_1 g}$	[1, 2]
Gravity	Bending rigidity	$(Eh^2/\rho_s g)^{1/3}$ or $(Er^2/\rho_s g)^{1/3}$	[146, 147]
Fluid inertial drag	Bending rigidity	$(Eh^3/\rho_l U^2)^{1/3}$	[148]
Fluid viscous drag	Bending rigidity	$(Er^3/\eta\omega)^{1/4}$	[148]
Bending rigidity	Thermal fluctuations	$Er^4/k_B T$	[101]

References

- [1] Adamson A W and Gast A P 1997 *Physical Chemistry of Surfaces* 6th edn (New York: Wiley-Interscience)
- [2] de Gennes P G, Brochard-Wyart F and Quéré D 2003 *Capillarity and Wetting Phenomena: Drops, Bubbles, Pearls, Waves* 1st edn (New York: Springer)
- [3] Madou M J 2002 *Fundamentals of Microfabrication: The Science of Miniaturization* 2nd edn (Boca Raton, FL: CRC Press)
- [4] Mastrangelo C H and Hsu C H 1993 Mechanical stability and adhesion of microstructures under capillary forces—part ii: experiments *J. Microelectromech. Syst.* **2** 33–43
- [5] Abe T and Reed M L 1996 Control of liquid bridging induced stiction of micromechanical structures *J. Micromech. Microeng.* **6** 213–6
- [6] Mayer T M, de Boer M P, Shinn N D, Clews P J and Michalske T A 2000 Chemical vapor deposition of fluoroalkylsilane monolayer films for adhesion control in microelectromechanical systems *J. Vac. Sci. Technol. B* **18** 2433–40
- [7] van Spengen W M, Puers R and De Wolf I 2002 A physical model to predict stiction in MEMS *J. Micromech. Microeng.* **12** 702–13
- [8] Raccurt O, Tardif F, Arnaud d'Avitaya F and Vareine T 2004 Influence of liquid surface tension on stiction of SOI MEMS *J. Micromech. Microeng.* **14** 1083–90
- [9] Tanaka T, Morigami M and Atoda N 1993 Mechanism of resist pattern collapse during development process *Japan. J. Appl. Phys.* **1** **32** 6059–64
- [10] Namatsu H, Kurihara K, Nagase M, Iwadata K and Murase K 1995 Dimensional limitations of silicon nanolines resulting from pattern distortion due to surface-tension of rinse water *Appl. Phys. Lett.* **66** 2655–7
- [11] Hui C Y, Jagota A, Lin Y Y and Kramer E J 2002 Constraints on microcontact printing imposed by stamp deformation *Langmuir* **18** 1394–407
- [12] Sharp K G, Blackman G S, Glassmaker N J, Jagota A and Hui C Y 2004 Effect of stamp deformation on the quality of microcontact printing: theory and experiment *Langmuir* **20** 6430–8
- [13] Tas N, Sonnenberg T, Jansen H, Legtenberg R and Elwenspoek M 1996 Stiction in surface micromachining *J. Micromech. Microeng.* **6** 385–97
- [14] Mastrangelo C H 1997 Adhesion-related failure mechanisms in micromechanical devices *Tribol. Lett.* **3** 223–38
- [15] Maboudian R and Howe R T 1997 Critical review: adhesion in surface micromechanical structures *J. Vac. Sci. Technol. B* **15** 1–20
- [16] Nguyen C V, Delzeit L, Cassell A M, Li J, Han J and Meyyappan M 2002 Preparation of nucleic acid functionalized carbon nanotube arrays *Nano Lett.* **2** 1079–81
- [17] Lau K K S, Bico J, Teo K B K, Chhowalla M, Amaratunga G A J, Milne W I, McKinley G H and Gleason K K 2003 Superhydrophobic carbon nanotube forests *Nano Lett.* **3** 1701–5
- [18] Chakrapani N, Wei B, Carrillo A, Ajayan P M and Kane R S 2004 Capillarity-driven assembly of two-dimensional cellular carbon nanotube foams *Proc. Natl Acad. Sci. USA* **101** 4009–12
- [19] Liu H, Li S H, Zhai J, Li H J, Zheng Q S, Jiang L and Zhu D B 2004 Self-assembly of large-scale micropatterns on aligned carbon nanotube films *Angew. Chem. Int. Edn* **43** 1146–9
- [20] Journet C, Moulinet S, Ybert C, Purcell S T and Bocquet L 2005 Contact angle measurements on superhydrophobic carbon nanotube forests: effect of fluid pressure *Europhys. Lett.* **71** 104–9
- [21] Dev A and Chaudhuri S 2007 Uniform large-scale growth of micropatterned arrays of ZnO nanowires synthesized by a surfactant assisted approach *Nanotechnology* **18** 175607
- [22] Fan J G, Dyer D, Zhang G and Zhao Y P 2004 Nanocarpet effect: pattern formation during the wetting of vertically aligned nanorod arrays *Nano Lett.* **4** 2133–8
- [23] Fan J G and Zhao Y P 2006 Characterization of watermarks formed in nano-carpet effect *Langmuir* **22** 3662–71
- [24] Chandra D, Taylor J A and Yang S 2008 Replica molding of high-aspect-ratio (sub-)micron hydrogel pillar arrays and their stability in air and solvents *Soft Matter* **4** 979–84
- [25] Chandra D and Yang S 2009 Capillary-force-induced clustering of micropillar arrays: is it caused by isolated capillary bridges or by the lateral capillary meniscus interaction force? *Langmuir* **25** 10430–4
- [26] Paulose J, Nelson D R and Aizenberg J 2010 Two-parameter sequential adsorption model applied to microfiber clustering *Soft Matter* **6** 2421–34
- [27] Otten A and Herminghaus S 2004 How plants keep dry: a physicist's point of view *Langmuir* **20** 2405–8
- [28] Bernardino N R, Blicke V and Dietrich S 2010 Wetting of surfaces covered by elastic hairs *Langmuir* **26** 7233–41
- [29] Fan J and Zhao Y 2010 Nanocarpet effect induced superhydrophobicity *Langmuir* **26** 8245–50
- [30] van Honschoten J W, Escalante M, Tas N R, Jansen H V and Elwenspoek M 2007 Elastocapillary filling of deformable nanochannels *J. Appl. Phys.* **101** 094310
- [31] van Honschoten J W, Escalante M, Tas N R and Elwenspoek M 2009 Formation of liquid menisci in flexible nanochannels *J. Colloid Interface Sci.* **329** 133–9
- [32] Tas N R, Escalante M, van Honschoten J W, Jansen H V and Elwenspoek M 2010 Capillarity negative pressure measured by nanochannel collapse *Langmuir* **26** 1473–6
- [33] van Honschoten J W, Brunets N and Tas N R 2010 Capillarity at the nanoscale *Chem. Soc. Rev.* **39** 1096–114
- [34] Yang Y, Gao Y F, Sun D Y, Asta M and Hoyt J J 2010 Capillary force induced structural deformation in liquid infiltrated elastic circular tubes *Phys. Rev. B* **81** 241407

- [35] Park K J and Kim H-Y 2008 Bending of floating flexible legs *J. Fluid Mech.* **610** 381–90
- [36] Vella D 2008 Floating objects with finite resistance to bending *Langmuir* **24** 8701–6
- [37] Eisner T and Aneshansley D J 2000 Defense by foot adhesion in a beetle (*Hemisphaerota cyanea*) *Proc. Natl Acad. Sci. USA* **97** 6568–73
- [38] Vogel S 2006 Living in a physical world VIII, gravity and life in water *J. Biosci.* **31** 309–22
- [39] Flynn M R and Bush J W M 2008 Underwater breathing: the mechanics of plastron respiration *J. Fluid Mech.* **608** 275–96
- [40] Halpern D and Grotberg J B 1992 Fluid-elastic instabilities of liquid-lined flexible tubes *J. Fluid Mech.* **244** 615–32
- [41] Clements J A 1997 Lung surfactant: a personal perspective *Annu. Rev. Physiol.* **59** 1–21
- [42] Heil M and White J P 2002 Airway closure: surface-tension-driven non-axisymmetric instabilities of liquid-lined elastic rings *J. Fluid Mech.* **462** 79–109
- [43] Hazel A L and Heil M 2005 Surface-tension-induced buckling of liquid-lined elastic tubes: a model for pulmonary airway closure *Proc. R. Soc. A* **461** 1847–68
- [44] Grotberg J B and Jensen O E 2004 Biofluid mechanics in flexible tubes *Ann. Rev. Fluid Mech.* **36** 121–47
- [45] Lester G R 1961 Contact angles of liquids at deformable solid surfaces *J. Colloid Sci.* **16** 315–26
- [46] Rusanov A I 1978 On the thermodynamic of deformable solid surfaces *J. Colloid Interface Sci.* **63** 330–45
- [47] Shanahan M E R and Carré A 1995 Viscoelastic dissipation in wetting and adhesion phenomena *Langmuir* **11** 1396–402
- [48] Carré A, Gastel J C and Shanahan M E R 1996 Viscoelastic effects in the spreading of liquids *Nature* **379** 432–4
- [49] Pericet-Camara R, Best A, Butt H-J and Bonaccorso E 2008 Effect of capillary pressure and surface tension on the deformation of elastic surfaces by sessile liquid microdrops: an experimental investigation *Langmuir* **24** 10565–8
- [50] Pericet-Camara R, Auernhammer G K, Koynov K, Lorenzoni S, Raiteri R and Bonaccorso E 2009 Solid-supported thin elastomer films deformed by microdrops *Soft Matter* **5** 3611–7
- [51] Yu Y-S and Zhao Y-P 2009 Elastic deformation of soft membrane with finite thickness induced by a sessile liquid droplet *J. Colloid Interface Sci.* **339** 489–94
- [52] Extrand C W and Kumagai Y 1996 Contact angles and hysteresis on soft surfaces *J. Colloid Interface Sci.* **184** 191–200
- [53] Carré A and Shanahan M E R 1997 Effect of cross-linking on the dewetting of an elastomeric surface *J. Colloid Interface Sci.* **191** 141–5
- [54] Sokuler M, Auernhammer G K, Roth M, Liu C, Bonaccorso E and Butt H-J 2010 The softer the better: fast condensation on soft surfaces *Langmuir* **26** 1544–7
- [55] Johnson K L, Kendall K and Roberts A D 1971 Energy and the contact of elastic solids *Proc. R. Soc. A* **324** 301–13
- [56] Landau L D and Lifshitz E M 1986 *Theory of Elasticity* 3rd edn (Oxford: Butterworth-Heinemann)
- [57] Timoshenko S P and Woinowsky-Krieger S 1959 *Theory of Plates and Shells* 2nd edn (Singapore: McGraw-Hill)
- [58] Py C, Reverdy P, Doppler L, Bico J, Roman B and Baroud C N 2007 Capillary origami: spontaneous wrapping of a droplet with an elastic sheet *Phys. Rev. Lett.* **98** 156103
- [59] Cohen A E and Mahadevan L 2003 Kinks, rings, and rackets in filamentous structures *Proc. Natl Acad. Sci. USA* **100** 12141–6
- [60] Zhou W, Huang Y, Liu B, Hwang K C, Zuo J M, Buehler M J and Gao H 2007 Self-folding of single- and multiwall carbon nanotubes *Appl. Phys. Lett.* **90** 073107
- [61] Cranford S, Sen D and Buehler M J 2009 Meso-origami: folding multilayer graphene sheets *Appl. Phys. Lett.* **95** 123121
- [62] Py C, Bastien R, Bico J, Roman B and Boudaoud A 2007 3D aggregation of wet fibers *Europhys. Lett.* **77** 44005
- [63] Kendall K 1971 The adhesion and surface energy of elastic solids *J. Phys. D: Appl. Phys.* **4** 1186–95
- [64] Kendall K 1976 Preparation and properties of rubber dislocations *Nature* **261** 35–6
- [65] Vella D, Bico J, Boudaoud A, Roman B and Reis P M 2009 The macroscopic delamination of thin films from elastic substrates *Proc. Natl Acad. Sci. USA* **106** 10901–6
- [66] Obreimoff J W 1930 The splitting strength of mica *Proc. R. Soc. A* **127** 290–7
- [67] Barthel E, Kerjan O, Nael P and Nadaud N 2005 Asymmetric silver to oxide adhesion in multilayers deposited on glass by sputtering *Thin Solid Films* **473** 272–7
- [68] Majidi C and Adams G G 2009 A simplified formulation of adhesion problems with elastic plates *Proc. R. Soc. A* **465** 2217–30
- [69] Majidi C and Adams G G 2010 Adhesion and delamination boundary conditions for elastic plates with arbitrary contact shape *Mech. Res. Commun.* **37** 214–8
- [70] Kim H Y and Mahadevan L 2006 Capillary rise between elastic sheets *J. Fluid Mech.* **548** 141–50
- [71] Tyree M T and Zimmerman M H 2002 *Xylem Structure and the Ascent of Sap* (New York: Springer)
- [72] Noblin X, Westbrook J, Rojas N, Argentina M and Dumais J 2009 Biomechanics of fern spores discharge: the sporangium opening *Proc. 6th Plant Biomechanics Conf. (Cayenne)* pp 179–86
- [73] Borno R T, Steinmeyer J D and Maharbiz M M 2006 Transpiration actuation: the design, fabrication and characterization of biomimetic microactuators driven by the surface tension of water *J. Micromech. Microeng.* **16** 2375–83
- [74] Bico J, Roman B, Moulin L and Boudaoud A 2004 Elastocapillary coalescence in wet hair *Nature* **432** 690
- [75] Liu J-L, Feng X-Q, Xia R and Zhao H-P 2007 Hierarchical capillary adhesion of microcantilevers or hairs *J. Phys. D: Appl. Phys.* **40** 5564–70
- [76] Kwon H-M, Kim H-Y, Puell J and Mahadevan L 2008 Equilibrium of an elastically confined liquid drop *J. Appl. Phys.* **103** 093519
- [77] Kim C-J, Kim J Y and Sridharan B 1998 Comparative evaluation of drying techniques for surface micromachining *Sensors Actuators A* **64** 17–26
- [78] Deladi S, Svetovoy V, Krijen G J M and Elwenspoek M C 2004 Flash release—an alternative for releasing complex MEMS devices *J. Micromech. Microeng.* **14** 1659–64
- [79] Hill J J, Haller K, Gelfand B and Ziegler K J 2010 Eliminating capillary coalescence of nanowire arrays with applied electric fields *Appl. Mat. Inter.* **2** 1992–8
- [80] Burns S J and Lawn B R 1968 A simulated crack experiment illustrating the energy balance criterion *Int. J. Fract. Mech.* **4** 339–45
- [81] Chopin J, Vella D and Boudaoud A 2008 The liquid blister test *Proc. R. Soc. A* **464** 2887–906
- [82] Hutchinson J W and Suo Z 1992 Mixed mode cracking in layered materials *Adv. Appl. Mech.* **29** 63–191
- [83] Mei Y, Thurmer D J, Cavallo F, Kiravittaya S and Schmidt O G 2007 Semiconductor sub-micro-/nanochannel networks by deterministic layer wrinkling *Adv. Mater.* **19** 2124–8
- [84] Annabattula R K, Veenstra J M, Mei Y F, Schmidt O G and Onck P R 2010 Self-organization of linear nanochannel networks *Phys. Rev. B* **81** 224114
- [85] Boudaoud A, Bico J and Roman B 2007 Elastocapillary coalescence: aggregation and fragmentation with a maximal size *Phys. Rev. E* **76** 060102
- [86] Pokroy B, Kang S H, Mahadevan L and Aizenberg J 2009 Self-organization of a mesoscale bristle into ordered, hierarchical helical assemblies *Science* **323** 237–40

- [87] Zhao Y P and Fan J G 2006 Clusters of bundled nanorods in nanocarpet effect *Appl. Phys. Lett.* **88** 103123
- [88] Chandra D and Yang S 2010 Stability of high-aspect-ratio micropillar arrays against adhesive and capillary forces *Acc. Chem. Res.* **43** 1080–91
- [89] Chaudhury M K, Weaver T, Hui C Y and Kramer E J 1996 Adhesive contact of cylindrical lens and a flat sheet *J. Appl. Phys.* **80** 30–7
- [90] Roca-Cusachs P, Rico F, Martínez E, Toset J, Farré R and Navajas D 2005 Stability of microfabricated high aspect ratio structures in poly(dimethylsiloxane) *Langmuir* **21** 5542–8
- [91] Geim A K, Dubonos S V, Grigorieva I V, Novoselov K S, Zhukov A A and Shapoval S Y 2003 Microfabricated adhesive mimicking gecko foot-hair *Nat. Mater.* **2** 461–3
- [92] Autumn K, Liang Y A, Hsieh S T, Zesch W, Chan W P, Kenny T W, Fearing R and Full R J 2000 Adhesive force of a single gecko foot-hair *Nature* **405** 681–5
- [93] Yao H and Gao H 2006 Mechanics of robust and releasable adhesion in biology: bottom-up designed hierarchical structures of gecko *J. Mech. Phys. Solids* **54** 1120–46
- [94] Bush J W M and Hu D L 2006 Walking on water: biolocomotion at the interface *Ann. Rev. Fluid Mech.* **38** 339–69
- [95] Neukirch S, Roman B, de Gaudemaris B and Bico J 2007 Piercing a liquid surface with an elastic rod: buckling under capillary forces *J. Mech. Phys. Solids* **55** 1212–35
- [96] Kornev K G, Callegari G, Kuppler J, Ruetsch S and Neimark A V 2006 Ribbon-to-fiber transformation in the process of spinning of carbon-nanotube dispersion *Phys. Rev. Lett.* **97** 188303
- [97] Chiodi F, Roman B and Bico J 2010 Piercing an interface with a brush: collaborative stiffening *Europhys. Lett.* **90** 44006
- [98] Wosten H A B, van Wetter M A, Lugones L G, van der Mei H C, Busscher H J and Wessels J G H 1999 How a fungus escapes the water to grow into the air *Curr. Biol.* **9** 85–8
- [99] Vollrath F and Edmonds T E 1989 Modulation of the mechanical properties of spider silk by coating with water *Nature* **340** 305–7
- [100] Marky N L and Manning G S 1991 The elastic resilience of DNA can induce all-or-none structural transitions in the nucleosome core particle *Biopolymers* **31** 1543–57
- [101] Schiessel H 2003 The physics of chromatin *J. Phys.: Condens. Matter* **15** R699–774
- [102] Bonaccorso E and Butt H-J 2005 Microdrops on atomic force microscope cantilevers: evaporation of water and spring constant calibration *J. Phys. Chem. B* **109** 253–63
- [103] Haschke T, Bonaccorso E, Butt H-J, Lautenschlager D, Schönfeld F and Wiechert W 2006 Sessile-drop-induced bending of atomic force microscope cantilevers: a model system for monitoring microdrop evaporation *J. Micromech. Microeng.* **16** 2273–80
- [104] Zheng X-P, Zhao H-P, Gao L-T, Liu J-L, Yu S-W and Feng X-Q 2008 Elasticity-driven droplet movement on a microbeam with gradient stiffness: a biomimetic self-propelling mechanism *J. Colloid Interface Sci.* **323** 133–40
- [105] Bowden N, Choi I S, Grzybowski B A and Whitesides G M 1999 Mesoscale self-assembly of hexagonal plates using lateral capillary forces: synthesis using the ‘capillary bond’ *J. Am. Chem. Soc.* **121** 5373–91
- [106] Green P W, Syms R R A and Yeatman E M 1995 Demonstration of three-dimensional microstructure self-assembly *J. Microelectromech. Syst.* **4** 170–6
- [107] Gracias D H, Kavthekar V, Love J C, Paul K E and Whitesides G M 2002 Fabrication of micrometer-scale, patterned polyhedra by self-assembly *Adv. Mater.* **14** 235
- [108] Syms R R A, Yeatman E M, Bright V M and Whitesides G M 2003 Surface tension-powered self-assembly of micro structures—the state-of-the-art *J. Microelectromech. Syst.* **12** 387–417
- [109] Boncheva M, Bruzewicz D A and Whitesides G M 2003 Millimeter-scale self-assembly and its applications *Pure Appl. Chem.* **75** 621–30
- [110] Mastrangeli M, Abbasi S, Varel C, Van Hoof C, Celis J-P and Boehringer K F 2009 Self-assembly from milli-to nanoscales: methods and applications *J. Micromech. Microeng.* **19** 083001
- [111] Leong T G, Zarafshar A M and Gracias D H 2010 Three-dimensional fabrication at small size scales *Small* **6** 792–806
- [112] van Honschoten J W, Berenschot J W, Ondarçuhu T, Sanders R G P, Sundaram J, Elwenspoek M and Tas N R 2010 Elastocapillary fabrication of three-dimensional microstructures *Appl. Phys. Lett.* **97** 014103
- [113] Cho J-H and Gracias D H 2009 Self-assembly of lithographically patterned nanoparticles *Nano Lett.* **9** 4049–52
- [114] Cho J-H, Azam A and Gracias D H 2010 Three-dimensional nanofabrication using surface forces *Langmuir* **26** 16534–9
- [115] Cho J-H, James T and Gracias D H 2010 Curving nanostructures using extrinsic stress *Adv. Mater.* **22** 2320–4
- [116] Guo X, Li H, Ahn B Y, Duoss E B, Hsia K J, Lewis J A and Nuzzo R G 2009 Two- and three-dimensional folding of thin film single-crystalline silicon for photovoltaic power applications *Proc. Natl Acad. Sci. USA* **106** 20149–54
- [117] Patra N, Wang B and Kral P 2009 Nanodroplet activated and guided folding of graphene nanostructures *Nano Lett.* **9** 3766–71
- [118] de Langre E, Baroud C N and Reverdy P 2010 Energy criteria for elasto-capillary wrapping *J. Fluid Struct.* **26** 205–17
- [119] Antkowiak A, Rivetti M, Audoly B, Neukirch S and Josserand C 2010 Instant capillary origami, in preparation
- [120] Piñeirua M, Bico J and Roman B 2010 Capillary origami controlled by electrowetting *Soft Matter* **6** 4491–6
- [121] Jung S, Reis P M, James J, Clanet C and Bush J W M 2009 Capillary origami in nature *Phys. Fluids* **21** 091110
- [122] Reis P M, Hure J, Jung S, Bush J W M and Clanet C 2010 Grabbing water *Soft Matter* **6** 5705–8
- [123] Yuan Q and Zhao Y-P 2010 Precursor film in dynamic wetting, electrowetting, and electro-elasto-capillarity *Phys. Rev. Lett.* **104** 246101
- [124] Armstrong J E 2002 Fringe science: are the corollas of Nymphaeoides (Menyanthaceae) flowers adapted for surface tension interactions? *Am. J. Bot.* **89** 362–5
- [125] Pocivavsek L, Dellsy R, Kern A, Johnson S, Lin B, Lee K Y C and Cerda E 2008 Stress and fold localization in thin elastic membranes *Science* **320** 912–6
- [126] Huang J, Davidovitch B, Santangelo C, Russel T P and Menon N 2010 Smooth cascade of wrinkles at the edge of a floating elastic film *Phys. Rev. Lett.* **105** 038302
- [127] Huang J, Juszkievicz M, de Jeu W H, Cerda E, Emrick T, Menon N and Russell T P 2007 Capillary wrinkling of floating thin polymer films *Science* **317** 650–3
- [128] Cerda E, Ravi-Chandar K and Mahadevan L 2002 Wrinkling of an elastic sheet under tension *Nature* **419** 579–80
- [129] Fortes M A 1984 Deformation of solid surfaces due to capillary forces *J. Colloid Interface Sci.* **100** 17–26
- [130] Kern R 1992 Deformation of an elastic thin solid induced by a liquid droplet *Surf. Sci.* **264** 467–94
- [131] Olives J 1993 Capillarity and elasticity. The example of the thin plate *J. Phys.: Condens. Matter* **5** 2081–94
- [132] Métois J J 1991 Elastic straining of a thin graphite layer by a liquid droplet or a non-epitaxed Pb crystallite *Surf. Sci.* **241** 279–88
- [133] Huang J, Menon N and Russell T P 2010 *Soft Matter* at press
- [134] Struik D J 1988 *Lectures on Classical Differential Geometry* 2nd edn (New York: Dover)
- [135] Alben S and Brenner M P 2007 Self-assembly of flat sheets into closed surfaces *Phys. Rev. E* **75** 056113

- [136] Boncheva M, Andreev S A, Mahadevan L, Winkleman A, Reichman D R, Prentiss M G, Whitesides S and Whitesides G M 2005 Magnetic self-assembly of three-dimensional surfaces from planar sheets *Proc. Natl Acad. Sci. USA* **102** 3924–9
- [137] Hure J, Bico J and Roman B 2010 Wrapping an adhesive sphere with a sheet, in preparation
- [138] Noblin X, Yang S and Dumais J 2009 Surface tension propulsion of fungal spores *J. Exp. Biol.* **212** 2835–43
- [139] Aristoff J M, Duprat C and Stone H A 2010 Elastocapillary imbibition *Int. J. Non-Linear Mech.* at press (doi:10.1016/j.ijnonlinmec.2010.09.001)
- [140] Duprat C, Aristoff J M and Stone H A 2010 Dynamics of elastocapillary rise *J. Fluid Mech.* submitted
- [141] Cambeau T and Reyssat E 2010 Capillary rise in flexible channels, in preparation
- [142] Monaenkova D and Kornev K G 2010 Elastocapillarity: stress transfer through fibrous probes in wicking experiments *J. Colloid Interface Sci.* **348** 240–349
- [143] Lobkovsky A, Gentges S, Li H, Morse D and Witten T A 1995 Scaling properties of stretching ridges in a crumpled elastic sheet *Science* **270** 1482–5
- [144] Ben Amar M and Pomeau Y 1997 Crumpled paper *Proc. R. Soc. A* **453** 729–55
- [145] Witten T A 2007 Stress focusing in elastic sheets *Rev. Mod. Phys.* **79** 643–75
- [146] Gordon J E 1991 *Structures* 1st edn (London: Penguin Books)
- [147] Vogel S 2006 Living in a physical world VII, gravity and life on the ground *J. Biosci.* **31** 201–14
- [148] Vogel S 1994 *Life in Moving Fluids* 2nd edn (Princeton: Princeton University Press)